CZECH TECHNICAL UNIVERSITY IN PRAGUE

FACULTY OF MECHANICAL ENGINEERING

DOCTORAL THESIS STATEMENT

CZECH TECHNICAL UNIVERSITY IN PRAGUE
Faculty of Mechanical Engineering
DEPARTMENT OF FLUID DYNAMICS AND THERMODYNAMICS

Summary of Dissertation Thesis

Synthetic and continuous jets impinging on a circular cylinder: Flow field and heat transfer experimental study

Zuzana Broučková

Doctoral Study Programme: *Mechanical Engineering*

Study Field: *Thermomechanics and fluid mechanics*

Supervisor: *Prof. Ing. Pavel Šafařík, CSc.*

Dissertation thesis statement for obtaining the academic title of "Doctor" abbreviated to "Ph.D."

Prague *January 2018*

Title in Czech language:

Syntetizovaný a kontinuální proud dopadající na kruhový válec: experimentální výzkum proudového pole a přestupu tepla

This doctoral thesis is an outcome of a full-time doctoral study programme at the Department of Fluid Dynamics and Thermodynamics, Faculty of Mechanical Engineering, Czech Technical University in Prague.

Disertant: Ing. Zuzana Broučková
Department Fluid Dynamics and Thermodynamics
Faculty of Mechanical Engineering,
Czech Technical University in Prague
Technická 4, 166 07 Prague 6, Czech Republic

Supervisor: prof. Ing. Pavel Šafařík, CSc.
Department Fluid Dynamics and Thermodynamics
Faculty of Mechanical Engineering,
Czech Technical University in Prague
Technická 4, 166 07 Prague 6, Czech Republic

Supervisor Specialist: doc. Ing. Zdeněk Trávníček, CSc.
Department Thermodynamics, Institute of Thermomechanics of the Czech Academy of Sciences
Dolejškova 1402/5, 182 00 Prague 8, Czech Republic

Reviewers:

The thesis was set out on:

The defense of the dissertation thesis will take place on:

The thesis is available in the Department od Science and Research of Faculty of Mechanical Engineering, CTU in Prague, Technická 4, Praha 6 - Dejvice.

prof. Ing. Jiří Nožička, CSc.
Head of Doctoral Study Field
Thermomechanics and fluid mechanics
Faculty of Mechanical Engineering CTU in Prague

Název práce: *Syntetizovaný a kontinuální proud dopadající na kruhový válec: experimentální výzkum proudového pole a přestupu tepla*

Anotace: V této práci byly zkoumány Syntetizovaný a kontinuální proud, které dopadaly na zahřívaný kruhový válec.
Práce byla experimentální. Pro tento účel byl navržen piezoelektrický generátor. Pracovním médiem byla voda. Základní parametry experimentu byly následující: šířka trysky byla 0,36 mm, poměr délky a šířky trysky byl 111, průměr válce byl 1,2 mm a vzdálenost mezi tryskou a válcem vztažená na šířku štěrbiny byla 5-21.
Experimentální vyšetřování proudového pole a přestupu tepla bylo provedeno za použití rozličných nezávislých metod. Při vyšetřování proudového pole byly použity tři optické metody: kvalitativní vizualizace pomocí metody laserem indukované fluorescence (laser induced fluorescence, LIF), laserová dopplerovská vibrometrie (laser Doppler vibrometry, LDV) a integrální laserová anemometrie (particle image velocimetry, PIV). Souběžně s optickými experimenty byl vyhodnocován celkový přestup tepla z kruhového válce.
Experimenty s přestupem tepla byly validovány režimem přirozené konvekce, kdy byla dosažena dobrá shoda s relevantními daty z dostupné literatury. Bylo zjištěno zvýšení Nusseltova čísla 4,2 až 6,2krát při použití syntetizovaného proudu oproti režimu přirozené konvekce. Byla navržena kriteriální rovnice pro průměrné Nusseltovo číslo platná pro syntetizovaný i kontinuální proud.

Title: *Synthetic and continuous jets impinging on a circular cylinder: Flow field and heat transfer experimental study*

Abstract: Synthetic and continuous jets impinging onto a heated circular cylinder were investigated.
The study was performed experimentally. For this reason, a piezoelectrically driven actuator with water as the working fluid was designed. The basic parameters of the experiments were: the slot nozzle width was 0.36 mm, the aspect ratio of the slot was 111, the cylinder diameter was 1.2 mm, and the cylinder-to-nozzle spacing related to the slot width was 5–21.
The experimental investigation of the flow field and heat transfer was performed by means of various independent methods. To investigate the flow field, three optical methods were used: qualitative laser-induced fluorescence (LIF) visualization, laser Doppler vibrometry (LDV) measurements, and particle image velocimetry (PIV) measurements. To investigate the heat

transfer, the overall convective heat transfer from the circular cylinder was evaluated, simultaneously with the optical experiments.

The heat transfer experiments were validated in a natural convection regime and reasonable agreement with representative references was concluded. An enhancement of the average Nusselt numbers by 4.2–6.2 times by means of the synthetic jets was quantified by comparison with the natural convection regime. A correlation for the average Nusselt number was proposed for both continuous and synthetic jets.

Contents

1. Introduction

The goal of this thesis is to describe the fluid mechanics and heat transfer of a fluid jet impinging on a circular cylinder, i.e., the flow of a submerged water jet originating from small-sized rectangular nozzles (less than 1 mm, i.e., micro-jet) and with a relatively high aspect ratio (higher than 100). Both synthetic (SJ) and conventional continuous (CJ) jets are investigated. The task is studied from a fluid mechanics and heat transfer point-of-view.

Generally speaking, CJ can be easily controlled. To facilitate investigations, some parts of complicated SJ experiments can be substituted by simpler CJ experiments. The hypothesis, which is the background for this approach, can be formulated according to the following three points:

- The behavior of CJ and SJ (e.g., regimes of flow separation on a cylindrical surface, including a jet splitting into two parts) are approximately (qualitatively) equivalent for identical Reynolds numbers.
- The average Nusselt number for CJ and SJ are determined by the Reynolds numbers and can be described by the same equations.
- The Reynolds number of SJ can be defined from the extrusion stroke of the SJ cycle.

This hypothesis is proposed considering current knowledge. There is no solution available in the literature yet. Moreover, results from macro-scale measurements cannot be used to corroborate micro-scale measurements. A typical example known from impinging CJs is the reduction in the stagnation Nusselt number resulting from a nozzle size decrease, at the same Reynolds numbers.

1.1 State of the art

1.1.1 Continuous jets

Free jet flows are jets which are not directly influenced by any walls. This category includes a free jet (a source of momentum), a plume (a source of buoyancy), a mixing layer and a wake flow [1,2]. The category of free jets includes free-surface jets and submerged jets (the submerged jet is a jet which is issuing into surroundings with approximately the same properties as the jet itself, typically water-to-water jet, air-to-air jet, etc.).

From a geometrical point-of-view, the two largest sub-categories of submerged jets are round (or axisymmetric) jets and plane jets (those originate from long slot orifices or nozzles).

Considering this terminology, the present study deals with submerged jets issuing from a slot nozzle in general, and with these jets impinging onto a circular cylinder.

1.1.1.1 Rectangular turbulent jets

To achieve a truly 2D plane jet is practically impossible in real-world devices. The ideal plane jet streams from a slot of infinite length. In the experimental praxis, the plane jets are usually realized by means of rectangular slots with high aspect ratios (AR), i.e., the ratio between the lengths of a long and a short side of the slot. Because the AR can never reach infinity, finite slot length generate so-called end-effects, which include the mixing and entrainments along the short sides of the slot (contrary to the pure 2D case). Other specific features result from the edge effects. The mixing-layers along the edges of the slot meet, interact and merge, which brings about new jet phenomena. Finally, a 3D jet character is developed.

The general properties of the rectangular turbulent jets were investigated by many authors, see e.g., Trentacoste and Sforza [3], Lemieux and Oosthuizen [4], Namer and Ötügen [5], Deo et al. [6], just to name a few.

Rectangular jets without sidewalls are often connected to an axis-switching, i.e., a three-dimensional deformation of the jet cross section due to jet spreading in the major- and minor-axis planes (see Trentacoste and Sforza [3]) and a saddle-back velocity profile phenomena (Vouros et al. [7]).

1.1.1.2 Microjets and very low Reynolds number jets

The term "microjet" is used to express small cross-section jet sizes – usually when at least one dimension is lower than 1 mm, see Cabaleiro and Aider [8]. One of the earlier studies, which considered the problem of microjets (in the contemporary terminology) and low Reynolds-number jets was performed by Sato and Sakao [9]. However, probably the first experimental study focusing exclusively on fundamental features of this phenomenon was introduced by Gau et al. [10].

1.1.2 Synthetic jets

A synthetic jet (SJ) is a reversible pulsating jet that is generated from fluid oscillations during a periodic fluid exchange between an actuator cavity and its surroundings. A typical SJ actuator has a cavity with an oscillating wall (diaphragm or piston). The cavity is opened to its surroundings via some orifice or nozzle (see e.g. [11,12]). The topic of rectangular SJ was studied e.g. in [11,13,14].

An interesting application field of the SJ is convective heat-transfer augmentation, e.g. [13,15-18]. A majority of these studies have focused on

air SJ impinging on a wall. An interesting up-to-date problem is the cooling of highly loaded electronic components in micro-channels, e.g., see Lee et al. [19] and Trávníček et al. [20].

1.1.3 Convective heat transfer

The topic of jets is closely bounded to the topic of convective heat transfer, particularly when the jets interact with solid body surfaces. Two main subcategories of convection can be distinguished: free convection (a fluid motion is driven by density gradients that produce a buoyancy force) and forced convection (a fluid motion is produced by an external source).

Impinging jets (IJs) are capable of achieving the highest forced convection heat/mass transfer rate between a single-phase fluid flow and a solid wall. Therefore, the IJs attracted attention in many heat/mass transfer studies.

For CJ impingement heat transfer from circular cylinders see e.g. [21-24].

The impinging SJs and heat transfer from a flat surface (plate) to the SJ were investigated in many studies. Surprisingly, there is (to the best of author's knowledge) no study dealing with heat transfer from a cylinder using SJ.

1.2 Aims of the dissertation

Based on the literature review the following aims of the dissertation were specified. The existing device, which was previously only preliminarily tested from the heat transfer point-of-view, will be modified and used for an experimental research. The aims of this dissertation is to experimentally solve the following three problems:

(1) Describe the behavior of synthetic jet (SJ) from the fluid mechanics point-of-view. Namely, to describe the behavior of a submerged SJ originating from a rectangular slot with small slot width (and associated Reynolds numbers), i.e., a (micro) SJ with a slot width below 1 mm.

(2) Describe the behavior of an SJ impinging onto a horizontal cylinder from the fluid mechanics and heat transfer point-of-view. Comparison of SJs and continuous jets (CJs) based on a hypothesis of their similarity.

(3) Quantify the overall convective heat transfer rates in terms of the average Nusselt and Reynolds numbers, i.e., to propose a new correlation equation.

More specifically, the three aims will be solved through the following particular tasks:

(1) The SJ will be investigated using water as the working fluid. The submerged SJ will be generated by a piezo-electrically driven actuator. The following experimental methods will be used: flow visualization (LIF, Laser

Induced Fluorescence), flow velocity measurement (PIV, Particle Image Velocimetry), surface velocity measurement (LDV, Laser Doppler Vibrometry), temperature point measurements (thermocouples and Pt100 probes).

The experiments will consist of an adequate preparation (including a state-of-the-art study of problems and methods), data acquisition, data processing, and result analysis including a comparison with available literature.

(2) A choice of operating parameters of the piezo-electrically driven SJs depends on the actuator's resonant behavior. Therefore, adjustments of the frequency and amplitude of the fluid oscillations are coupled with and related to a particular transducer.

(3) Heat transfer experiments will include an overall convective heat transfer measurement based on the Joule effect (the heat generated by the electric current flowing through a conductor). A validation should be based on representative references, therefore the natural convection from cylinders will be used. New correlation equations for the average Nusselt number will be proposed.

2. Experimental setup

The experimental device is shown in Fig. 1 (including the coordinate system). The used device was previously patented [25] and preliminarily studied from the heat transfer point-of-view. The actuator body is made up of PMMA (polymethyl methacrylate). It is equipped with a piezoelectric diaphragm (1) (KPS-l00 piezoceramic transducer). The diaphragm consists of a central piezoceramic part (25 mm in diameter and total thickness of 0.22 mm) bonded to a brass part (0.11 mm thick). The diameter of the flexible metal diaphragm, rounded with a plastic rim, is $D_D = 39.5$ mm. The actuator body and the diaphragm create a cavity (2) with a diameter and depth of 44 mm and 6 mm, respectively. The jet flow is ejected from a slot (3) on the top of the cavity. The slot width and length are $B = 0.36$ mm and $L_s = 40$ mm, respectively. Thus, the aspect ratio of the slot is $AR = L_s/B = 111$. The length of the nozzle exit channel is $L = 1.0$ mm.

The actuator can operate in two regimes: it can produce either a continuous jet (CJ) or a synthetic jet (SJ). When the device is operated in the CJ regime, the fluid is fed into the cavity of the actuator using a centrifugal pump (Atman AT-301). The pump is connected to the actuator via a flexible pipe and the fluid enters the cavity opposite to the center of the piezoelectric diaphragm (4). The pump is placed either in the same tank as the actuator or in a separate tank. The former arrangement is used for PIV experiments, the

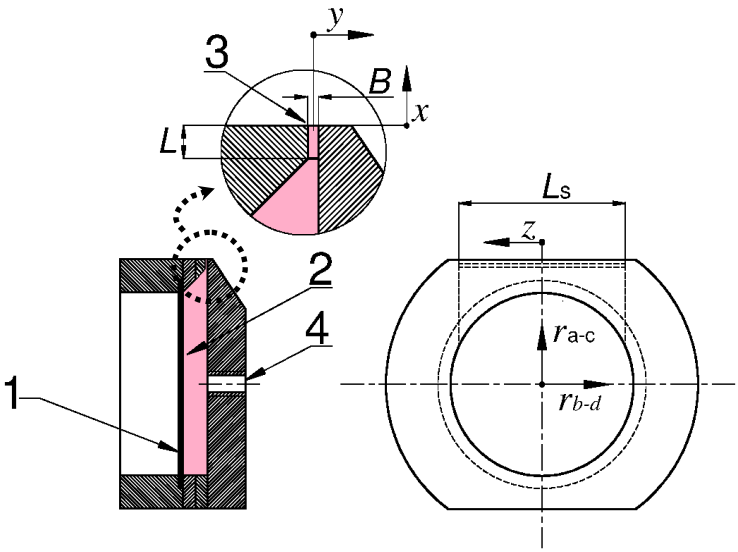

Fig. 1 Schematic view of the experimental device;
1: piezoelectric diaphragm, 2: cavity, 3: nozzle, 4: water pump inlet.

latter for LIF visualization and for evaluation of the time-mean volume flux by means of the gravimetric method (via the precise scales). Under the CJ regime, the piezoceramics transducer is not fed.

When the device operates as an SJ actuator, the inlet from the pump is sealed and the piezoceramics diaphragm is driven by the sinusoidal current from a sweep/function generator (Agilent 33210A), which is amplified by an amplifier (RH Sound ST2250BC).

The setup used for the work with the SJ actuator during the PIV measurement of the flow-field without the cylinder is slightly different: the sinusoidal signal is generated by the function generator (Wavetek model 395) which is amplified by the amplifier (Krohn-Hite model 7602M).

Figure 2 shows an overall scheme of the experimental setup, including the cylinder downstream from the nozzle, which was designed for heat transfer measurements. The cylinder (1) is made up of a smooth stainless steel tube; its outside and inside diameters are D = 1.21 mm and 0.91 mm, respectively. The cylinder is mounted parallel to the actuator slot. It is fastened into place by two metal brackets (2). The total cylinder length is the distance between the brackets, L_C = 57.5 mm.

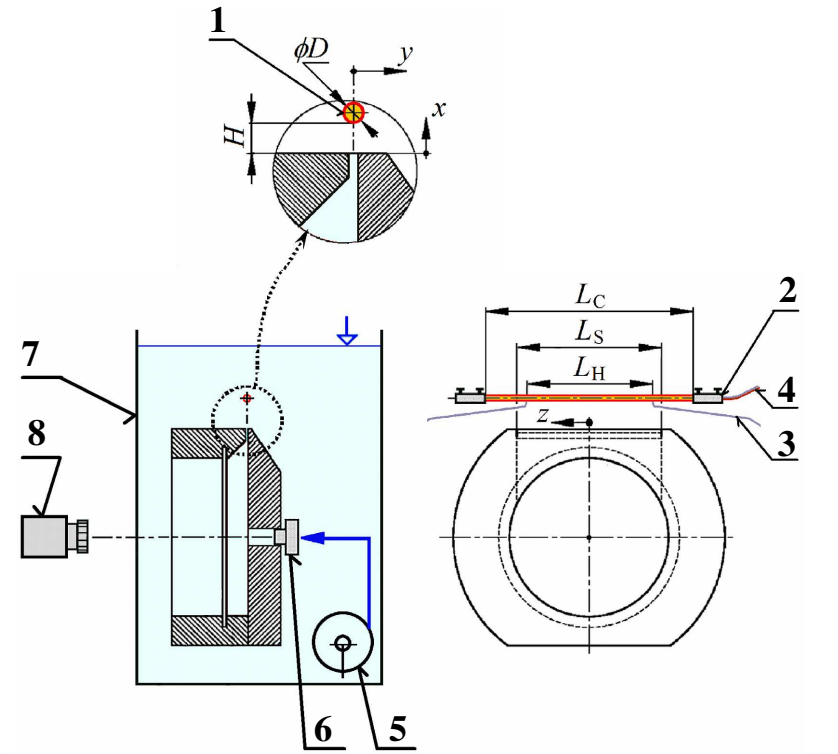

Fig. 2 The overall scheme of the experiment;
1: cylinder, 2: cylinder brackets, 3: stainless steel wires (measurement of voltage difference), 4: thermocouple, 5: centrifugal pump, 6: plug, 7: glass tank, 8: vibrometer (LDV).

For heat transfer experiments, the cylinder is heated via the Joule effect of direct current I_c from the brackets. The test section is in the middle part of the cylinder, which is defined by contact points with a span of L_H = 35.3 mm. In these contact points the stainless steel wires with diameter 0.20 mm (3) are welded and the voltage difference V_c is measured between them. The cylinder end-parts, from the test section, operate as end-guard sections. This arrangement minimizes axial conduction-based heat losses from the test section.

Most of the SJ experiments were made with a drive frequency of f = 46 Hz. A typical RMS voltage was V_{SJ} = 18.0 V. For this supply, the electrical power was approximately P_{SJ} = 17 mW.

3. Experimental methods

3.1 Laser induced fluorescence (LIF)

In the present study, the LIF technique was used for visualization of the flow field. Rhodamine B was chosen as the fluorescent dye. The experiments were made in a glass water tank that had dimensions: height × length × depth = 150 × 245 × 140 mm and that was filled with pure water.

When the SJA is operated in the CJ regime, the pump is placed in a separate tank. The separate tank is then filled with dye solution. Subsequently, the pump is turned on. When the SJA is operated in the SJ regime, the cavity of switched-off actuator is filled with the dye. Consequently, the actuator is placed into the tank filled with water and it is switched on. In both cases (CJ and SJ), the dye-stained flow is lit by a laser sheet perpendicular to the slot, i.e., in the *x*–*y* or *x*-*z* plane (along the slot), see Fig. 3.

The pictures of the visible flow field pattern (streaklines) are taken using a high resolution digital camera. To remove the laser light from the pictures, a color filter (cut-off wavelength 570 nm) is used. The camera is used to trigger the laser pulse. The measurement system is controlled via DynamicStudio v3.40 Software (Dantec Dynamics).

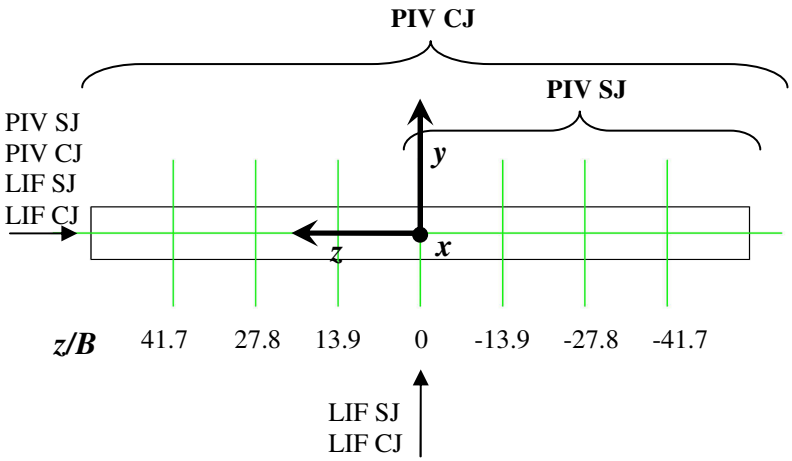

Fig. 3 Schematic view on the exit slot (from the top) with planes where the LIF visualization and PIV measurement were performed.

3.2 Particle image velocimetry (PIV)

PIV experiments of the flow-field *without a cylinder* were done in the National Taiwan University, Institute of Applied Mechanics laboratory – see Broučová et al. [26]. The experiments were performed in a cubic glass water tank with the side length of 390 mm. The PIV system (using Dantec Dynamics, FlowMap1500) was used with polyamide seeding particles (5 μm in diameter). The light source was a Nd:YAG dual laser head system with a cylindrical lens. The image pairs were acquired using a CCD camera. The typical time delay between pulses was in the range 700 to 3000 μs. The pictures were taken using Flow Manager software (Dantec Dynamics). The subsequent post-processing was done using DynamicStudio v3.40 Software (Dantec Dynamics).

The velocity vectors were calculated using an advanced cross-correlation technique, namely the DynamicStudio built-in Adaptive PIV technique. This method iteratively adjusts the size and shape of the individual IA to adapt local seeding densities and gradients (for more details, see [27]). The minimum size of the IA was 32 × 32 pixels and the maximum size was 64 × 64 pixels, with a grid step size of 16 × 16 pixels with 50% overlap and a moving average area filtered via a 3 × 3-pixel window. Velocity and vorticity maps were averaged from a sequence of approximately 100 images. The experiments were performed as the phase-locked measurement, after the periodic nature of the SJ.

Investigations of the flow-field *within the cylinder* were performed using the PIV system in Prague, at IT CAS. The experiments were performed with the same setup described above (3.1 LIF visualization method). The fluorescence particles (1–20 μm in diameter) were used. The images were post-processed via DynamicStudio v5.1 software (Dantec Dynamics). The procedure and the software setup was same as the previous test.

Both visualization using LIF and PIV measurements were performed on several planes. The schematic illustration of the individual laser sheet positions is shown in Fig. 3.

3.3 Laser Doppler vibrometry (LDV)

Measurement of the oscillating piezoceramics diaphragm velocity was performed. The LDV technique was used. A portable digital vibrometer (Ometron VH-1000-D, B&K 8338) was used in this study [28]. The typical sampling frequency and number of samples are 10 kHz and 16,384, respectively. The procedure for data post processing, including phase averaging, was developed in MATLAB (for more details, see Broučková et al. [28]).

During the experiments, the SJ actuator was placed in a glass water tank filled with pure water, then the SJ actuator was switched on. The laser beam was focused on the rear of the piezoceramic diaphragm. The velocity waveforms were investigated in the centre of the diaphragm and in another 8 points at diameters of 20 mm and 34 mm.

By using LDV, the velocity waveforms at the selected points of the diaphragm were measured, phased-averaged and consequently integrated to obtain the time behavior of the deflected surface during the period. Knowing the deflections of 9 points on the surface, the evolution of the diaphragm shape during one actuation period was determined. Considering the slug-flow (one-dimensional or "piston-like" flow) model for fluid flow through the SJ slot nozzle, the harmonic motion of the diaphragm results in a harmonic motion of the fluid through the nozzle outlet, so the instantaneous velocity in the nozzle outlet is

$$u_0(t) = U_{\max} \sin(\varphi), \tag{1}$$

where $U_{\max}$ is the maximum SJ velocity at the nozzle outlet. By using the continuity equation for incompressible flow, the maximum flow velocity can be express by

$$U_{\max} = 2c\pi f y_{\max}\left(\frac{A_D}{A_s}\right), \tag{2}$$

where A_D is the diaphragm area ($A_D = \pi D_D^2/4$), A_S is the cross-sectional area of the slot nozzle ($A_S = BL_s$), and c is the parameter that considers the diaphragm shape.

3.4 Gravimetric method

Due to micro-size and expected low velocity of the CJ, the gravimetric method was used to evaluate the time-mean volume flux of the CJ. The experiment was made using precise laboratory scales (Mettler Toledo PR 8002 Delta Range) with the resolution 0.01 g. The amount of water discharged during the specified time (typically 3–10 min) was weighed and consequently the average volume flux Q, through the nozzle, was evaluated. The time and spatial mean velocity at the nozzle exit U_m was evaluated via the equation

$$U_m = \frac{Q}{L_s B}. \tag{3}$$

3.5 Temperature measurement

The cylinder temperature, T_w, was measured using a J type thermocouple and an Omega DP41-B thermometer. The thermocouple was plugged into the cylinder tube. The bulk temperature of water T_∞ was measured by an NTC thermistor sensor (Ahlborn AMR, Therm 2280-3).

All experiments were made after a thorough stabilization of the temperatures. In this study, the temperature ranged between approximately T_w = 20.8–40 °C and T_∞ = 20.8–26.8°C, depending on the adjusted heating power.

4. Relevant parameters

4.1 Continuous jet

The Reynolds number of the jet is usually based on the width of slot B and the mean velocity at the exit slot U_m:

$$Re_{CJ} = \frac{BU_m}{\nu}, \tag{4}$$

where ν is the kinematic viscosity. When the obstacle is placed in the flow (cylinder in this case), scaling of the additional independent Reynolds number with the dimension of the obstacle (the diameter of the cylinder D) is possible via the expression

$$Re_{CJ,D} = \frac{DU_m}{\nu}. \tag{5}$$

4.2 Synthetic jet

The Reynolds number of the synthetic jet is often based on the time-average velocity at the exit orifice obtained from the extrusion part of the period T_E (modified from [11]), U_0

$$U_0 = \frac{1}{T}\int_0^{T_E} u_0(t)dt, \tag{6}$$

where $T = 1/f$ is the duration of a single period and f is the jet frequency. When the slug flow model is considered, the velocity U_0 can be evaluated from its instantaneous velocity on the jet axis at the nozzle exit, u_0 (see Eq. (1)). When Eq. 1 is obeyed (i.e., the waveform is purely sinusoidal), the relation $U_{max} = \pi U_0$ is valid. The Reynolds number of the SJ can be defined (similarly to Eqs. 4 and 5 for CJs):

$$Re_{SJ} = \frac{BU_0}{\nu} \tag{7}$$

and

$$Re_{SJ,D} = \frac{DU_0}{\nu}. \tag{8}$$

4.3 Heat transfer

The governing parameters for the forced convection are the Reynolds and the Prandtl numbers, $Pr = \nu/\alpha$ (α is the thermal diffusivity). For the natural convection, the governing parameters are the Grashof number ($Gr = g\beta(T_w - T_\infty)D^3/\nu^2$, where g is the acceleration of gravity, β is the volumetric thermal expansion coefficient) and the Prandtl number [29].

In general, (if the compressibility or high velocities are not considered) the overall convective heat transfer is expressed by the following equation ([30]):

$$Nu = f\left(Gr, Pr, Re, T_w / T_\infty\right), \tag{9}$$

where Nu is the average Nusselt number over the entire cylindrical circumference, T_w is the (surface) wall temperature, and T_∞ is the bulk (ambient) temperature. The average Nusselt number is defined as

$$Nu = \frac{hD}{k}, \tag{10}$$

where h is the average heat transfer coefficient, D is the characteristic dimension (here the cylinder diameter) and k is the thermal conductivity of the fluid.

5. Results and analysis

5.1 Continuous jet (CJ)

5.1.1 Evaluation of the time-mean exit velocity

Following the approach described previously, the time-mean volume flux of the CJ was evaluated using the laboratory scales. The measurement was performed for three volume fluxes. The results are summarized in Table 1.

Table 1 Parameters of the CJ experiments

Q l/min	U m/s	Re_{CJ}
0.090	0.10	40
0.177	0.20	79
0.357	0.41	161

The measurement was performed three times for each case. The values in Table 1 are the average values of all three measurements. The Reynolds numbers for all three cases are higher than the limit for laminar jet flows reported by Blevins [2] ($Re_{CJ} = 30$) or by Sato and Sakao [9] ($Re_{CJ} = 33$), thus the turbulent jet flow can be expected in the present CJ.

The CJ with the lowest Reynolds number ($Re_{CJ} = 40$) was chosen for more detailed investigation.

5.1.2 Continuous jet - flow visualization

The next step in the investigation of the CJ is the qualitative visualization of the flow field. Figure 4 shows a visualization of the CJ across the slot. The laser sheet was positioned at x-y plane, in the middle of the exit slot ($z = 0$). The instantaneous picture reveals that the jet keeps its initial nature for a great distance downstream; the jet only slightly gradually spreads in the lateral direction. On the contrary, only a slight contraction was found in the spanwise direction (not shown here). The jet is smooth, with no visible coherent structures (i.e., vortex formation), breakdown and transition process which are typical for turbulent macro-jets. These observations agree with the micro-jet results by Gau et al. [10] - the dimensionless breakdown length according to [10] should be very far downstream at $L_b/B = 350$. This is far beyond the present field of view.

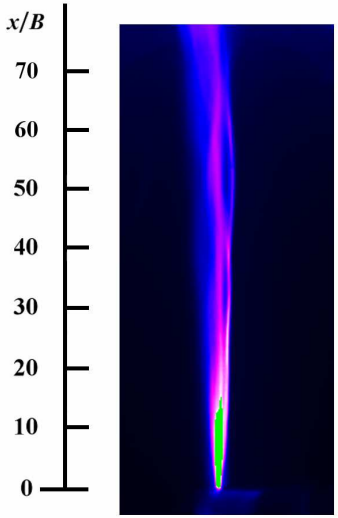

Fig. 4 Visualization of the CJ across the slot (x-y plane).

5.1.3 Continuous jet - PIV results

To explore the behavior of the jet in more detail, two vector maps are shown in Fig. 5. The measurement was performed across the slot, at the positions z/B = -41.7 (z = -15 mm, left picture) and 0 (z = 0, right pictures). These coordinates correspond to positions where the maximum and the minimum velocity were identified, i.e., where the one of the local maxima and the local minimum of the saddle-back profile are situated. The vectors are colored by the velocity magnitude $U_{x\text{-}y}$ (a) and by the vorticity ω_z (b). The velocity fields, in both locations, are qualitatively similar. The jet is acceptably symmetrical, although a slight asymmetry and deflection to the right is visible in the image from the middle of the slot. The width of the jet is also comparable in both cases. From a quantitative point-of-view, the pictures differ dramatically; as was expected from previous measurement results the velocities in the peak of the saddle shape (z/B = -41.7) are approximately 50% higher than in the central part (the local maximum $U_{x\text{-}y}$ = 0.055 m/s at the z/B = -41.7 against the local maximum $U_{x\text{-}y}$ = 0.024 m/s at the z/B = 0).

The corresponding streamlines for the flow-field from Figs. 5(a) and (b) are shown in Fig. 5(c) and confirms the smooth nature of the jet.

From all the PIV measurement results some observations can be summarized:

- The jet is smooth without the apparent coherent structures and no turbulent transition was observed in this case although the Reynolds number could indicate the turbulent flow.
- Neither axis switching, nor gradual merging or disappearance of the side peaks were identified (these effects are usual for macro-jets e.g., [7]). The reasons are the quite high AR and the micro-size of the jet.

5.2 Synthetic jet (SJ)

5.2.1 Synthetic jet - LDV results

The time-mean exit velocity U_0 and the SJ Reynolds number were evaluated as U_0 = 0.18 m/s and Re_{SJ} = 67. A significant local velocity maximum in the frequency characteristic was found at f = 46.4 Hz (U_0 = 0.18 m/s). For most experiments the frequency f = 46 Hz was chosen.

5.2.3 Synthetic jet - flow visualization

Figure 6 shows the visualization across the slot in the middle of the nozzle approximately in the middle of the extrusion phase of the working cycle. Three subsequent vortex pairs are clearly visible. The third one starts the breaking-up process and will merge with the previously extruded vortex puffs in the next parts of the cycle. When compared with the CJ (see Fig. 4), the SJ

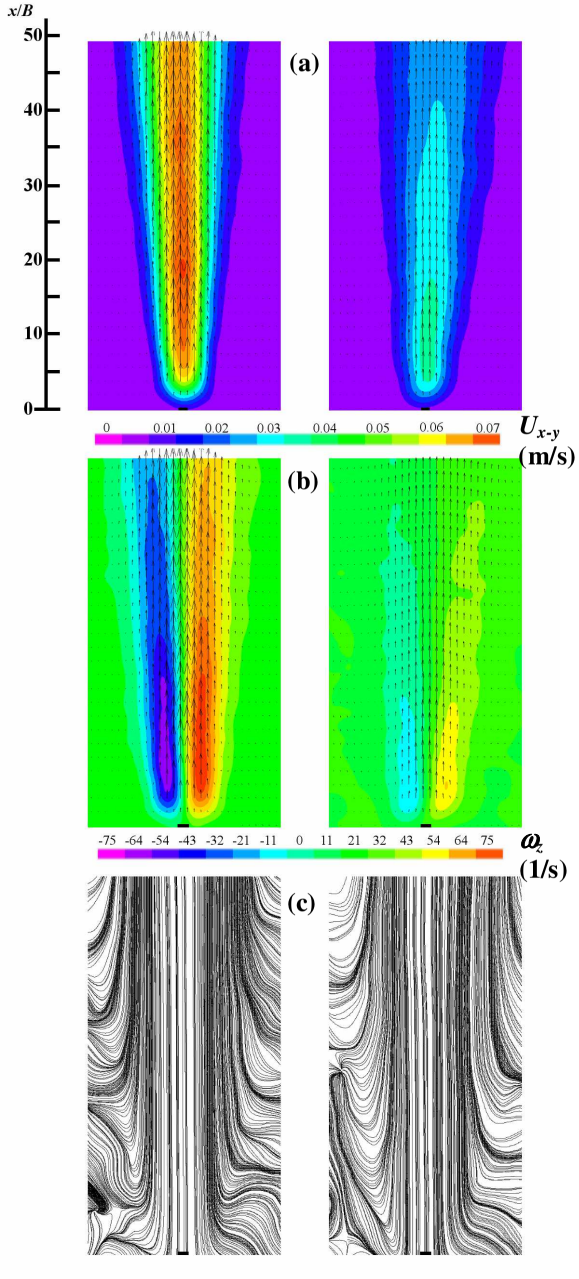

Fig. 5 Velocity vector field of the CJ across the slot (x-y plane) at z/B = -41.7 (left) and 0 (right) colored by (a) Velocity magnitude, (b) Vorticity and (c) Corresponding streamlines.

is wider and the width of the jet grows gradually from the beginning to the distance around $x/B = 30$, where the jet breaks up and its width increases distinctly. This contrasts with the smooth and slowly changing CJ, which does not break up in the observed area.

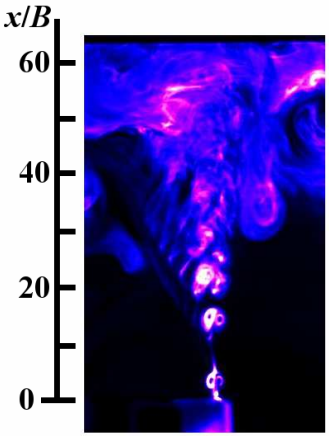

Fig. 6 Visualization of the SJ across the slot (*x*-*y* plane).

5.2.4 Synthetic jet - PIV results

Unlike the steady CJ, the SJ experiments require to be performed in space and also in time, i.e., at several phases of the cycle. For this reason, eight phase-locked measurements, with the equidistant phase step of $t/T = 0.125$, (i.e. $\varphi = 45°$) were performed at every investigated position.

Figure 7 shows the vector fields of the SJ at $z/B = 0$ in the middle of the extrusion stroke (left picture) and in the middle of the suction stroke (right picture) colored with the velocity magnitude $U_{x\text{-}y}$ and with the vorticity ω_z and the corresponding streamlines. The formation of the extruded vortex pair is visible during the suction stroke and on the contrary, the reverse direction of the velocity vectors during the suction is apparent in the right picture. The existence of three separate vortex pairs can be observed during the extrusion, during the suction, the upper vortex lost its coherence and merges around $x/B = 15$–20 with previously extruded fluid puffs and cannot be distinguish anymore. The position of the break up agrees well with the corresponding visualization from Fig. 6. After the break-up of the coherent vortex structures the jet become non-symmetrical, and it is split into two streams; the prevailing amount of the fluid continues straightly downstream and the minor part of the jet is deflected to the left. The position where the jet width increases, reasonably corresponds to the initialization of the break-up. This observation is in accordance with previous findings by Amitay and Cannelle [14].

The time-mean velocity profiles were calculated from the measured phase-locked velocity profiles and the 3D contours map of the time-mean streamwise velocity components are shown in Fig. 8(a). For comparison purposes, the 3D-contour graphs of the CJ are plotted in Fig. 8(b) as well. Both jets are strongly influenced by near-end effects and the existence of the

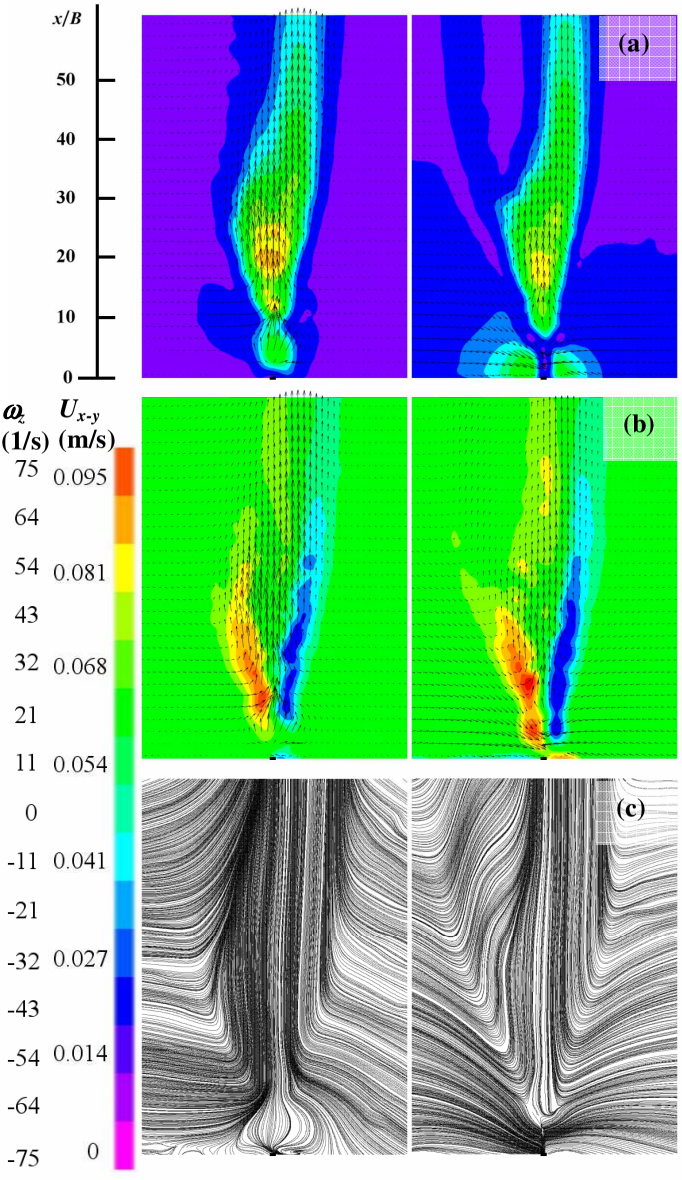

Fig. 7 Velocity vector field of the SJ across the slot (x-y plane) at $z/B = 0$ and $\varphi = 90°$ (left) and 270° (right) colored by
(a) Velocity magnitude, (b) Vorticity and (c) Corresponding streamlines.

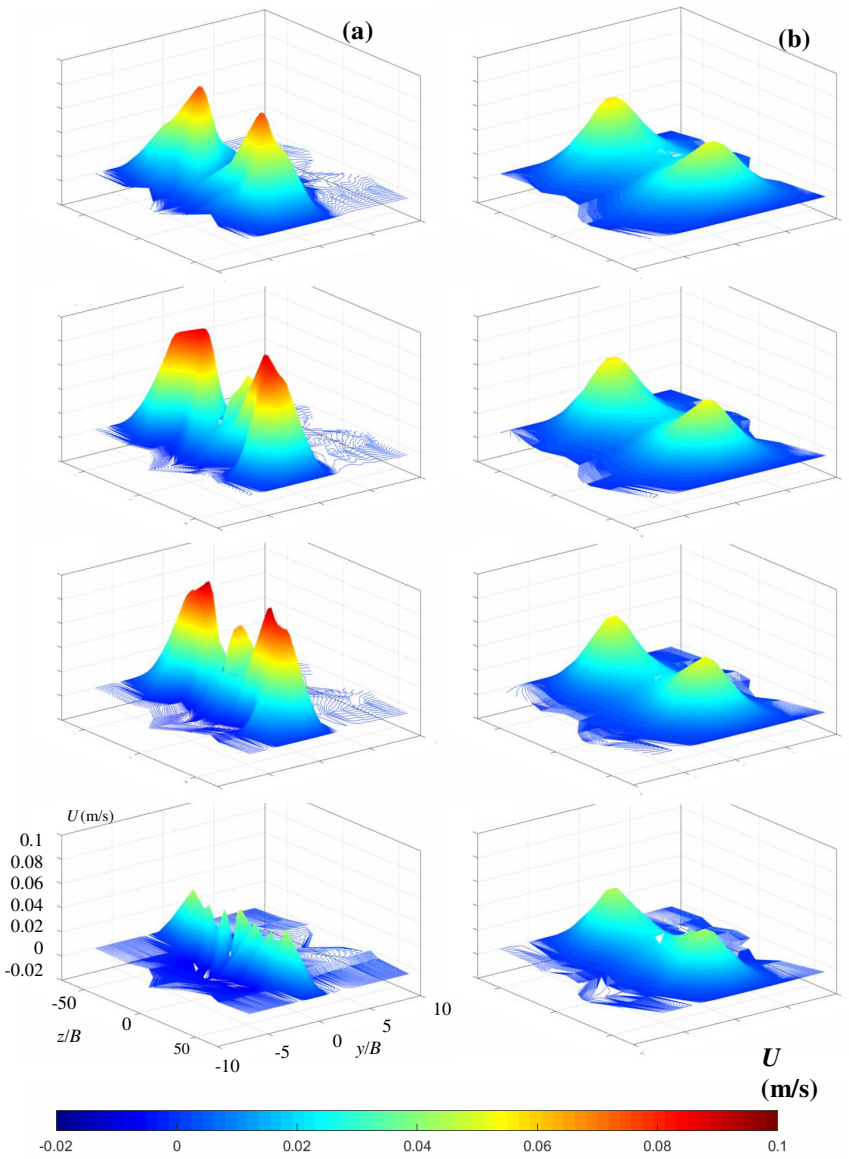

Fig. 8 3D contours of the time-mean streamwise velocity component
(a) SJ
(b) CJ.

pair of off-axis peaks is evident. The formation of the peaks is faster in the CJ case. There are peaks that are already formed at $x/B = 10$, while a series of several smaller peaks can be observed for SJ. The existence of the row of small peaks of the SJ at $x/B = 10$ is related to "streaky-like" structures that are finer, not organized in the near-field and become well-organized further downstream. The "streaky-like" character of the SJ also initializes the formation of the middle peak, which is not present for CJ. However, with the increasing distance from the nozzle exit, the end effects begin to dominate, the middle peak is shifted along the y-axis and gradually diminishes. The position of the peaks remains almost unchanged in the CJ case (around $z/B = \pm 40$) but varies with distance in the SJ case (from $z/B = \pm 25$ to ± 35). The change of the position is not monotonic; however, the peaks are always placed symmetrically. The unsteady character of SJ along with a "streaky-like" structure causes a less symmetrical, less "smooth" and less organized velocity field in SJ compared to CJ.

5.3 The jet impinging onto the cylinder

In the next step, the cylinder was placed downstream of the nozzle (see Fig. 2) and the basic characteristics of the flow-field with obstacle were investigated. The preliminary results have been published recently [31,32].

In Table 2, the experimental settings for both CJ and SJ are summarized (the settings for the CJ corresponds to the values shown in Table 1, the SJ is the nominal case).

Table 2 Parameters of the experiments - CJ and SJ impinging onto the cylinder

	Q l/min	f Hz	P_{SJ} mW	U m/s	U_0 m/s	Re_{CJ}	Re_{SJ}	$Re_{CJ,D}$	$Re_{SJ,D}$	Re_{DC}
CJ	0.090			0.10		40		135		102
	0.177			0.20		79		267		203
	0.357			0.41		161		542		412
SJ		46	17		0.18		67		225	171

As the initial step, the selected cases were visualized and they are shown in Fig. 9 and 10. The actuator slot is on the bottom margin of the images, and the orifice-to-cylinder spacing was adjusted as $H = 20.8B$. Based on the flow visualization results shown in Figs. 9 and 10, three main effects can be distinguished:

- The Reynolds number effect is demonstrated via a comparison of Figs. 9(a) and 9(b). Both jets are identical in character (CJs) and identical in thermal conditions (unheated, i.e., $T_w = T_\infty$.). The Reynolds number is

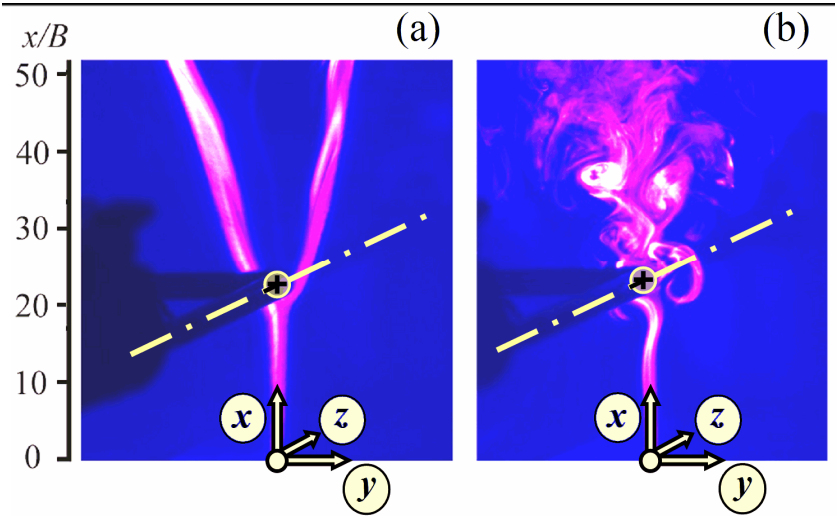

Fig. 9 LIF visualization of the CJs, unheated cases at $T_w = T_\infty$ and $H/B = 20.8$ for (a) $Re_{CJ} = 40$ (i.e., $Re_{CJ,D} = 135$),
(b) $Re_{CJ} = 161$ (i.e., $Re_{CJ,D} = 542$).

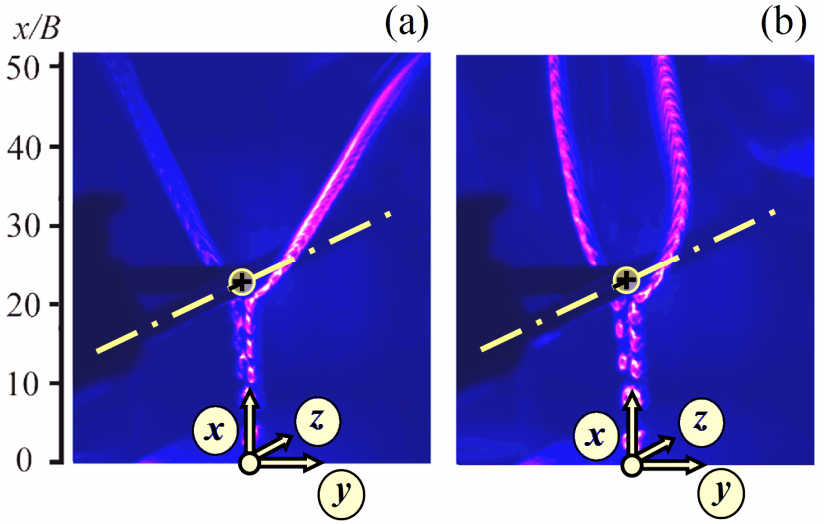

Fig. 10 LIF visualization of the SJs, $Re_{SJ} = 67$, $H/B = 20.8$
(a) Unheated case,
(b) Heated case at $T_w = 28.4$°C and $T_\infty = 22.8$°C.

increased from $Re_{CJ} = 40$ (i.e., $Re_{CJ,D} = 135$, Fig. 9(a)) to $Re_{CJ} = 161$ (i.e., $Re_{CJ,D} = 542$, Fig. 9(b)). Fig. 9(a) shows the CJ impinging on the cylinder. From the stagnation zone, the jet is divided into two halves. A flow separation occurs very soon on the windward cylinder side. Finally, the flow leaves the cylinder in two halves, forming a Y-shaped pattern. The flow around the leeward cylinder side is weak (not visible in Fig. 9(a)), which indicates a highly probable decrease in the overall heat transfer rate. Probable reasons are effects of the mini scale and the low Reynolds numbers. Conversely, the flow pattern is different for greater $Re_{CJ,D}$ values, as shown in Fig. 9(b). Unlike Fig. 9(a), the flow around the leeward cylinder side exists in Fig. 9(b). The flow pattern resembles a vortex-shedding wake known for cylinders in a cross-flow.

- The thermal effect is demonstrated via a comparison of Figs. 10(a) and 10(b). Again, for comparison purposes, both jets are identical in character (SJs) and the $Re_{SJ} = 67$ is identical as well. While Fig. 10(a) shows the unheated cylinder case, the heated cylinder case is shown in Fig. 10(b) and has the temperatures $T_w = 28.4°C$ and $T_\infty = 22.8°C$. For both cases, the SJ impinges on the cylinder surface and is divided into two halves. A flow separation occurs very soon on the windward cylinder side and the flow leaves the cylinder in two halves, forming a Y-shaped pattern. The flow around the leeward cylinder side was weak and not visible in both cases (i.e., Figs. 10(a) and 10(b)). Note some specific features of the heated cylinder case in Fig. 10(b). While both branches of the Y-shaped flow leaving the cylinder for the unheated cases in Fig. 10(a) are straight and directed nearly tangentially from the cylinder surface, these flow branches from the heated cylinder in Fig. 10(b) are curved towards each other. This thermal effect in the far field indicates a thermal plume that is released from the leeward cylinder side where the forced jet flow does not reach. Obviously, the thermal plume is not visible.
- The effect of the jet's nature is demonstrated via a comparison of Figs. 9(a) and 10(a), respectively. Both unheated cylinder cases are different in terms of the nature of jets: CJ vs. SJ, respectively. Differences in the Reynolds numbers of the jets are not dominant: $Re_{CJ} = 40$ vs. $Re_{SJ} = 67$, respectively. The distinct character of the streaklines clearly indicates both jets: while the smooth streaklines in Fig. 9(a) indicate the CJ, a train of vortices in Fig. 10(a) is typical for the SJ. However, the dominant features of both cases are qualitatively similar as was described in the text above: the jet impingement and division into two halves, flow separation on the windward cylinder side, and two jet halves leaving the cylinder as the Y-shaped pattern.

5.4 Convective heat transfer - forced convection

After the natural convection validation experiment, the forced convection investigation was performed.

Figure 11 demonstrates the heat transfer enhancement by means of the SJ at $H/B = 10$. It is obvious that the SJ causes the Nusselt number to enhance by 4.2–6.2 times against the natural convection. Moreover, Fig. 11 demonstrates the uncertainty of the experiments via the error bars indicating the expanded uncertainties of the 95 % confidence level (i.e., ±2 standard deviations σ_{Nu}). Obviously, the experiments with larger heating inputs and higher $T_w - T_\infty$ differences have smaller uncertainties (the error bars cannot be visible in Fig. 11 because they are smaller than the data marks). On the other hand, the forced convection of smaller input heating and lower $T_w - T_\infty$ have higher uncertainties. For example, SJ experiments for $P < 0.8$ W have $T_w - T_\infty < 1$ °C and uncertainties $2\sigma_{Nu} > 18$ %; such experiments are qualitative only and they are omitted from data processing. Nevertheless, the results of these experiments are also plotted in Fig. 11 to demonstrate these effects.

In the next step the effect of the nozzle-to-cylinder spacing H/B was investigated while the Reynolds number was kept approximately constant ($Re_{CJ,D}$, $Re_{SJ,D}$ = 220-270), see Fig. 12. The effect of the H/B spacing on Nu appears to be negligible, which agrees with the literature for lower Reynolds

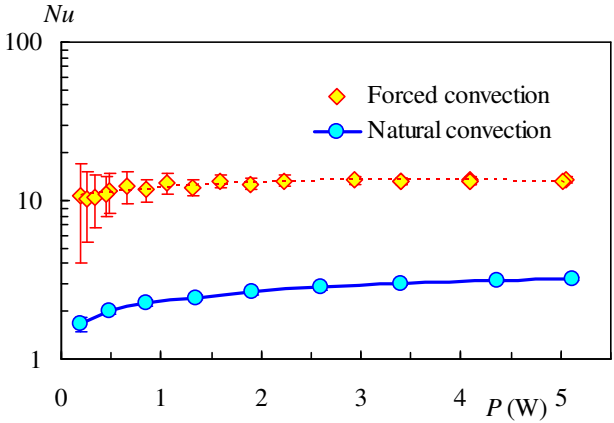

Fig. 11 Comparison of the natural and forced convection (SJ, $H/B = 10$); the error bars indicate the expanded uncertainties with a 95% confidence level (i.e. ±2 standard deviation σ_{Nu}).

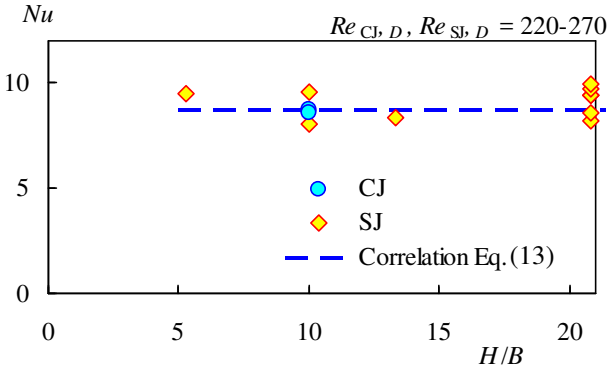

Fig. 12 Effect of the nozzle-to-cylinder spacing on *Nu*.

numbers (cf. Jeng et al. [33], for $Re_D < 1300$). The dashed line representing Eq. (13) is also plotted in Fig. 12, it will be described and explained in the text below.

Figure 13(a) shows the present forced convection data. For comparison, two references are used that relate to the heat transfer from a circular cylinder to a uniform cross-flow (Morgan [30]) and to an IJ (Amiri et al. [24]). Note that Amiri et al. [24] are the only authors from the list of available literature that fit the range of Reynolds number investigated in this work; moreover, the comparison of the present results with the data by Amiri et al. [24] is still very rough because no results exist in the available literature with closer parameters, namely with small cylinders (1 mm order of magnitude of diameters) in a jet flow. The Nusselt numbers for the present CJ and SJ were evaluated at temperature T_w, which was measured at the center plane $z = 0$. Additionally, the data series labeled as "CJ, near-end data" uses a *Nu* evaluation from T_w, which was measured at the end of the cylinder test section where the local maximum of the CJ velocity occurs; see Fig. 8. Obviously, the near-end *Nu* values were greater than *Nu* values for the center plane. The reason is the saddle-back velocity profile. Namely, the mean center plane exit velocity is smaller than the mean exit velocity U, whereas the near-end exit velocity is higher. To quantify this effect, the $C(z)$ factor is defined as the ratio of the exit velocity in the z location to the mean exit velocity U_m, i.e.,

$$C(z) = u(x=0, y=0, z) / U_m. \quad (11)$$

This factor was evaluated for the saddle-back velocity profiles at $x/B = 10–40$ for z-locations at the center plane where $z = 0$ and the near-end plane where

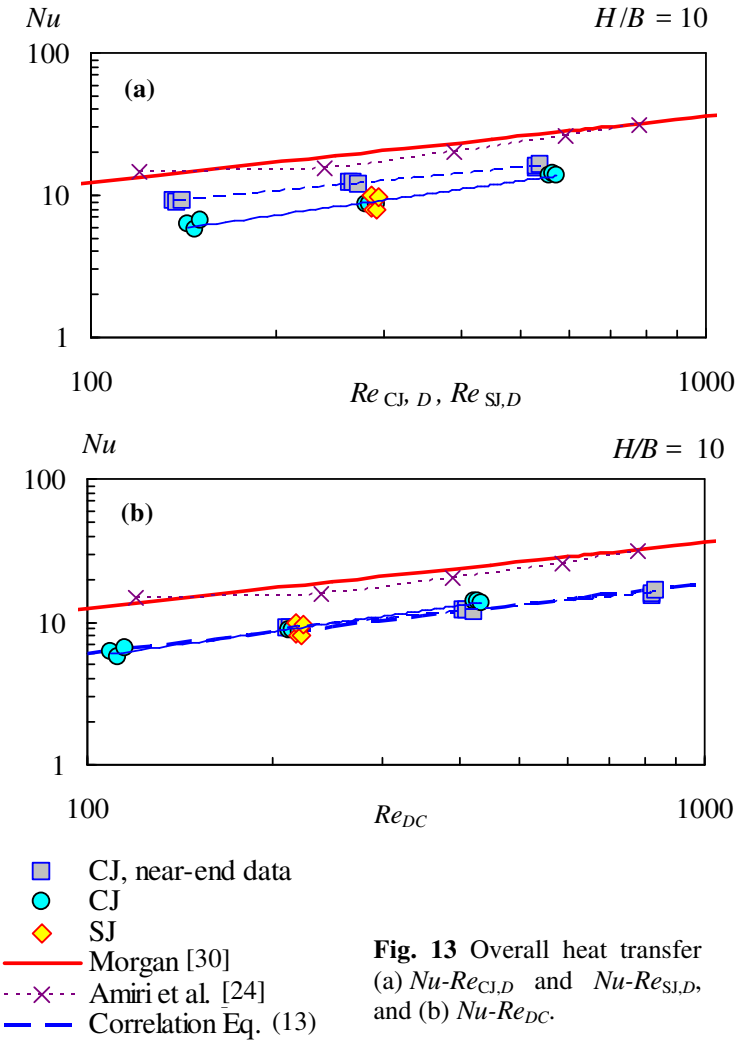

Fig. 13 Overall heat transfer (a) Nu-$Re_{CJ,D}$ and Nu-$Re_{SJ,D}$, and (b) Nu-Re_{DC}.

z = 15 mm. The resulting values are $C(z=0) = 0.76 \pm 0.06$ and $C(z=15$ mm$) = 1.55 \pm 0.06$. Finally, the C factor was used to correct the Reynolds number for the center plane conditions via

$$Re_{DC} = C \cdot Re_{CJ,D}. \qquad (12)$$

Considering the described corrections, the results from Fig. 13(a) are replotted in Fig. 13(b) as the Nu-Re_{DC} relationship. By using a least-squares fitting, the results were correlated via

$$Nu = 0.63\ Re_{DC}^{0.49}, \tag{13}$$

for Re_{DC} = 110–830. The maximum and standard deviation of the experimental data from Eq. (13) are 13% and 7%, respectively.

Figure 13(b) demonstrates similar slopes for all correlation lines, i.e., a qualitative agreement of the present data with the correlation performed by Morgan [30] (who proposed the exponent of 0.471). However, the present Nu values were much smaller than the results of [24,30], approximately 50% of their results. The present smaller Nu values are a manifestation of the flow patterns discussed above when only a relatively small windward side the cylinder circumference is effectively cooled by the jet and flow separation occurs there – see the flow visualizations in Figs. 9 and 10. The reasons for this result are a combination of the mini-scale effect from the narrow slot (B = 0.36 mm), the relatively small B/D ratio, and the relatively low Re_D with a prevailing laminar flow character. However, the choice of small values for B, B/D and Re_D follows the requirements for potential applications on mini/micro scales, even though this choice reduces the Nusselt number compared with a cylinder in an infinite uniform cross-flow and significantly saves the volume flux of the cooling fluid. A small volume flux is a principal capability of very compact, piezoelectric-driven actuators. Moreover, scaling down this alternative appears to be possible, compared with the classical, compressor-driven macro scale devices investigated in [24,30] because neither a pump (a blower), nor fluid supply piping is required.

6. Conclusions

6.1 Results and contribution of the thesis

This experimental work dealt with submerged water micro jets (the width of the jet is B = 0.36 mm) issuing from a rectangular nozzle with a relatively higher aspect ratio (AR = 111) at lower Reynolds numbers (Re = 40–160). The focus was given on a piezo-electrically driven synthetic jet. For comparison purposes, the continuous jet issuing from the same facility was also investigated. The task was studied from a fluid mechanics and heat transfer point-of-view.

In the Introduction part of the thesis, three aims were given. The fulfillment of the objectives is summarized in the following list:

(1) Fluid mechanics of a synthetic jet (SJ) issuing from a rectangular slot with

small Reynolds numbers and small slot width – namely, the (micro) SJ with a slot width below 1 mm.

First, an extensive literature review was performed. Consequently, the free submerged synthetic jet was generated using a piezo-electrically driven actuator (Re_{SJ} = 67). The actuator was operated close to its resonant frequency (f = 46 Hz). The flow field was investigated using flow visualization (LIF technique) and velocity measurement (PIV technique). The time-mean output velocity was evaluated using surface measurements of a diaphragm deflection (LDV technique).

The present measurements revealed the highly 3D character of the initially rectangular jet. The strong variation of the velocity magnitude along the nozzle span was observed. The existence of streaky-like patterns in the velocity/vorticity field was confirmed. The present results are in good agreement with data from available literature.

(2) Fluid mechanics and heat transfer characteristics of the SJ impinging on a horizontal cylinder. A comparison of SJs and CJs is based on a hypothesis of their similarity.

The continuous jets were investigated at Re_{CJ} = 40, 79, 161 and the basic characteristics of the flow-fields were compared with data from available literature. The highly 3D nature of the initially 2D jet was revealed. The dependence of the velocity field on the spanwise location was identified. Saddle back velocity profiles were observed - as expected.

On the other hand, no gradual merging of the peaks or axis switching was revealed in this case. The results agree with the literature for common macro jets. Moreover, some findings relate to the micro-size of the present jet, thus neither large coherent structures nor break-up effects were identified. The low mixing intensity and a slow axis velocity decrease were found.

- The synthetic jet was compared to continuous (steady) jets and several similarities were found in terms of the time-mean characteristics: highly 3D character of the jet issuing from a rectangular slot, highly non-uniform velocity distribution along the span and an absence of the axis switching phenomenon. Visualization of both continuous and synthetic jets impinging onto a circular cylinder confirms the expected flow-field similarity in this case, i.e., both jets are split into two halves after hitting the cylinder surface.
- The overall heat transfer characteristics were evaluated for both the continuous and synthetic jets impinging onto the cylinder. The average Nusselt numbers are commensurate in both cases. A quantification of the results was concluded by a proposal of a new correlation equation, as described in point 3.

- To determine synthetic jets, the Reynolds number was defined from the extrusion stroke of the cycle. The suitability of this approach for fluid mechanics and heat transfer components of the problem was confirmed.

(3) Quantification of the overall convective heat transfer rate in terms of the average Nusselt and Reynolds numbers.

To validate present overall convective heat transfer measurement, the natural convection from cylinders was measured. The results are in excellent agreement with representative references.

The enhancement of the average Nusselt number, using both continuous and synthetic jet, against natural convection was found to be 4.2–6.2 times. The influence of the nozzle-to-cylinder distance on the average Nusselt number was found to be negligible. The Nusselt number obtained for the present microjet was lower than the Nusselt number for conventional macro jet. A new correlation equation for the present range of parameters was proposed: $Nu = 0.63\ Re_D^{0.49}$.

The results of the thesis contribute to

- deepening the basic knowledge of synthetic jet behavior from a fluid mechanics and heat transfer point-of-view,
- establishing more precise background for future investigations of potentially suitable cooling alternatives (e.g., highly loaded up-and-coming electronic components).

6.2 Future work

The future work could incorporate several of the following suggestions:

The present synthetic jet actuator can be optimized. The optimal working parameters to reach the maximal heat transfer rate and/or maximal efficiency can be found. An advanced variant of the actuator geometry with fluidic diodes (i.e., hybrid synthetic jet) could be applied.

Another important point that is admittedly far beyond the fluid mechanic and heat transfer point-of-view, is the design and utilization of more efficient piezoceramic transducers. Just note here that the present study used an available piezoceramic transducer, which is (in principle) not appropriate for underwater use.

Finally, the future work could and should apply more advanced measurement techniques and technologies. For example, the used experimental methods did not allow an investigation in the very nearfield of the jets. The present experiments focused on the time-mean and phase-averaged characteristics,

which revealed many interesting features of the flow-fields and heat transfer mechanisms. However, advanced measurement technologies, with finer scaling in the spatial and time domains, could provide more valuable results. The use of micro-PIV and time-resolved PIV techniques can bring deeper sights into the physics of the micro-synthetic jets.

References

[1] H. Schlichting, K. Gersten, Boundary-Layer Theory, Springer-Verlag, Berlin (2000).

[2] R.D. Blevins, Applied Fluid Dynamics Handbook, Krieger Publ. Comp., Malabar, Florida (2003).

[3] N. Trentacoste, P. Sforza, Further Experimental Results for Three-Dimensional Free Jets, AIAA Journal 5 (5) (1967) 885-891.

[4] G.P. Lemieux, P.H. Oosthuizen, Experimental Study of the Behavior of Plane Turbulent Jets at Low Reynolds Numbers, AIAA Journal 23 (12) (1985) 1845-1846.

[5] I. Namer, M.V. Ötügen, Velocity Measurement in a Plane Turbulent Air Jet at Moderate Reynolds Numbers, Experiments in Fluids 6 (1988) 387-399.

[6] R.C. Deo, J. Mi, G.J. Nathan, The Influence of Nozzle Aspect Ratio on Plane Jets, Experimental Thermal and Fluid Science 31 (2007) 825-838.

[7] A.P. Vouros, T. Panidis, A. Pollard, R.R. Schwab, Near Field Vorticity Distributions from a Sharp-Edged Rectangular Jet, International Journal of Heat and Fluid Flow 51 (2015) 383-394.

[8] J.M. Cabaleiro, J.-L. Aider, Axis-Switching of a Micro-Jet, Physics of Fluids 26 (2014).

[9] H. Sato, F. Sakao, An Experimental Investigation of the Instability of a Two-Dimensional Jet at Low Reynolds Numbers, Journal of Fluid Mechanics 20, part 2 (1964) 337-352.

[10] C. Gau, C.H. Shen, Z.B. Wang, Peculiar Phenomenon of Micro-Free-Jet Flow, Physics of Fluids 21 (2009) 1-13.

[11] B.L. Smith, A. Glezer, The Formation and Evolution of Synthetic Jets, Physics of Fluids 10 (1998) 2281–2297.

[12] J.E. Cater, J. Soria, The Evolution of Round Zero-Net-Mass-Flux Jets, Journal of Fluid Mechanics 472 (2002) 167–200.

[13] M.B. Gillespie, W.Z. Black, C. Rinehart, A. Glezer, Local Convective Heat Transfer from a Constant Heat Flux Flat Plate Cooled by Synthetic Air Jets, Transactions ASME Journal of Heat Transfer 128 (2006) 990–1000.

[14] M. Amitay, F. Cannelle, Evolution of Finite Span Synthetic Jets, Physics of Fluids 18 (2006) 054101.

[15] Z. Trávníček, V. Tesař, Annular Synthetic Jet Used for Impinging Flow Mass–Transfer, International Journal of Heat and Mass Transfer 46 (2003) 3291–3297.

[16] D.S. Kercher, J.-B. Lee, O. Brand, M.G. Allen, A. Glezer, Microjet Cooling Devices for Thermal Management of Electronics, IEEE Transactions on Components Packaging and Manufacturing Technology 26 (2) (2003) 359–366.

[17] R. Mahalingam, N. Rumigny, A. Glezer, Thermal Management Using Synthetic Jet Ejectors, IEEE Transactions on Components Packaging and Manufacturing Technology 27 (3) (2004) 439–444.

[18] T. Persoons, A. McGuinn, D.B. Murray, A General Correlation for the Stagnation Point Nusselt Number of an Axisymmetric Impinging Synthetic Jet, International Journal of Heat and Mass Transfer 54 (2011) 3900–3908.

[19] A. Lee, V. Timchenko, G.H. Yeoh, J.A. Reizes, Three-Dimensional Modelling of Fluid Flow and Heat Transfer in Micro-Channels with Synthetic Jet, International Journal of Heat and Mass Transfer 55 (2012) 198–213; Erratum in International Journal of Heat and Mass Transfer 55 (2012) 2746.

[20] Z. Trávníček, P. Dančová, J. Kordík, T. Vít, M. Pavelka, Heat and Mass Transfer Caused by a Laminar Channel Flow Equipped with a Synthetic Jet Array, Transactions ASME Journal of Thermal Science and Engineering Applications 2 (2012) 041006-1–041006-8.

[21] H. Schuh, B. Persson, Heat Transfer on Circular Cylinders Exposed to Free-Jet Flow. International Journal of Heat and Mass Transfer 7 (1964) 1257-1271.

[22] C.S. McDaniel, B.W. Webb, Slot Jet Impingement Heat Transfer from Circular Cylinder, International Journal of Heat and Mass Transfer 43 (2000) 1975–1985.

[23] E.M. Sparrow, A. Alhomoud, Impingement Heat Transfer at a Circular Cylinder due to an Offset or Non-Offset Slot Jet, International Journal of Heat and Mass Transfer 27 (12) (1984) 2297-2306.

[24] S. Amiri, K. Habibi, E. Faghani, M. Ashjaee, Mixed Convection Cooling of a Heated Circular Cylinder by Laminar Upward-Directed Slot Jet Impingement. Heat and Mass Transfer 46 (2009) 225–236.

[25] Z. Trávníček, Z. Broučková, Způsob a zařízení pro chlazení těles válcového tvaru proudem chladicí tekutiny, CZ patent č. 306506 (2017).

[26] Z. Broučková, S.-S. Hsu, A.-B. Wang, Z. Trávníček, Water Synthetic Jet Driven by a Piezoelectric Actuator – LIF and PIV Experiments. Advanced Materials Research 1104 (2015) 45–50.

[27] Dynamic Studio, User's Guide, Dantec Dynamics.

[28] Z. Broučková, T. Vít, Z. Trávníček, Laser Doppler Vibrometry Experiment on a Piezo-Driven Slot Synthetic Jet in Water. The European Physical Journal, EPJ Web of Conferences 92 (2015) Article No. 02007, 1–7.

[29] F.P. Incropera, D.P. DeWitt, Introduction to Heat Transfer. 3rd Ed., John Wiley & Sons, New York (1996)

[30] V.T. Morgan, The Overall Convective Heat Transfer from Smooth Circular Cylinders, Advances in Heat Transfer 11 (1975) 199–264.

[31] Z. Broučková, Z. Trávníček, Visualization and Heat Transfer Study of a Synthetic Jet Impinging on a Circular Cylinder, in: Proceedings of 12th International Conference on Heat Transfer, Fluid Mechanics and Thermodynamics (HEFAT2016), Malaga, Spain (2016) 1791–1796.

[32] Z. Broučková, Z. Trávníček, T. Vít, Synthetic and continuous jets impinging on a circular cylinder, Heat Transfer Engineering 40 (13–14) (2019) (in press; on line version will be available in 2018).

[33] T.-M. Jeng, S.-C. Tzeng, R. Xu, Heat Transfer Characteristics of a Rotating Cylinder with a Lateral Air Impinging Jet, International Journal of Heat and Mass Transfer 70 (2014) 235–249.

Publications of author

Publications with the direct connection to the results of the thesis

Publications indexed in Web of Science and Scopus

Journal with impact factor

[ZB1] Z. Broučková, Z. Trávníček, T. Vít, Synthetic and continuous jets impinging on a circular cylinder. *Heat Transfer Eng.* 40 (13–14) 2019 (in press; on line version will be available in 2018).

Journals without impact factor

[ZB2] Z. Broučková, S.-S. Hsu, A.-B. Wang, Z. Trávníček, PIV and LIF study of slot continuous jet at low Reynolds number. EPJ Web of Conferences 114, 02007 (2016). (Experimental Fluid Mechanics 2015, Prague, Czech Republic).

[ZB3] Z. Broučková, T. Vít, Z. Trávníček, Laser Doppler vibrometry experiment on a piezo-driven slot synthetic jet in water. EPJ Web of Conferences 92 02007 (2015). (Experimental Fluid Mechanics 2014, Český Krumlov, Czech Republic).

Publications not indexed in WoS and Scopus

Journal without impact factor

[ZB4] Z. Broučková, S.-S. Hsu, A.-B. Wang, Z. Trávníček, Water synthetic jet driven by a piezoelectric actuator - LIF and PIV experiments. Advanced Materials Research 1104 (2015) 45-50. (Spring International Conference on Material Sciences and Technology 2015, Beijing, China).

Conference contribution

[ZB5] Z. Broučková, Z. Trávníček, Visualization and heat transfer study of a synthetic jet impinging on a circular cylinder. In: Proceedings of 12th International Conference on Heat Transfer, Fluid Mechanics and Thermodynamics /HEFAT2016/, Costa del Sol, Spain, 11-13 July 2016, pp. 1791-1796.

Publications without the direct connection to the results of the thesis

Publications indexed in Web of Science and Scopus

Journal with impact factor

[ZB6] Z. Broučková, P. Šafařík, Z. Trávníček, A parameter map of synthetic jet regimes based on the Reynolds and Stokes numbers: commentary on the article by Rimasauskiene et al. *Mech. Syst. Signal Proc.* 68-69 (2016) pp. 620-623

[ZB7] Z. Trávníček, Z. Broučková, J. Kordík, T. Vít, Visualization of synthetic jet formation in air. *J. Vis.* 18 (2015) pp. 595-609

[ZB8] Z. Broučková, Z. Trávníček, Visualization study of hybrid synthetic jets. *J. Vis*. 18 (2015) pp. 581-593

[ZB9] J. Kordík, Z. Broučková, Z. Trávníček, Impinging jet-based fluidic diodes for hybrid synthetic jet actuators. *J. Vis.* 18 (3) (2015) pp. 449-458

[ZB10] J. Kordík, Z. Broučková, T. Vít, M. Pavelka, Z. Trávníček, Novel methods for evaluation of the Reynolds number of synthetic jets. *Exp Fluids*. 55 (6) (2014) pp. 1757-1-1757-16.

[ZB11] Z. Trávníček, V. Tesař, Z. Broučková, K. Peszyński, Annular impinging jet controlled by radial synthetic jets. *Heat Transfer Eng*. 35 (16-17) (2014), pp. 1450-1461.

[ZB12] Z. Trávníček, Z. Broučková, J. Kordík, Formation criterion for synthetic jets at high Stokes numbers. *AIAA J*. 50 (9) (2012) pp. 2012-2017.

Journals without impact factor

[ZB13] Z. Broučková, Z. Trávníček, PIV and LIF study of flow and thermal fields of twine plumes in water. EPJ Web of Conferences 143 02012 (2017). (Experimental Fluid Mechanics 2016, Mariánské Lázně, Czech Republic).

[ZB14] Z. Broučková, E. Flídr, P. Šafařík, Z. Trávníček, Active control of the wake behind the cylinder. EPJ Web of Conferences 143 02011 (2017). (Experimental Fluid Mechanics 2016, Mariánské Lázně, Czech Republic).

[ZB15] Z. Broučková, P. Pušková, Z. Trávníček, P. Šafařík, Jet flow issuing from an axisymmetric pipe-cavity-orifice nozzle. EPJ Web

of Conferences 114, 02006 (2016). (Experimental Fluid Mechanics 2015, Prague, Czech Republic).

[ZB16] Z. Broučková, Z. Trávníček, P. Šafařík, Bubble dynamics in drinks. EPJ Web of Conferences 67 02011 (2014). (Experimental Fluid Mechanics 2013, Kutná Hora, Czech Republic).

[ZB17] Z. Broučková, Z. Trávníček, P. Šafařík, Active control of the jet in coaxial arrangement. EPJ Web of Conferences 45 01016 (2013). (Experimental Fluid Mechanics 2012, Hradec Králové, Czech Republic).

[ZB18] V. Tesař, Z. Broučková, J. Kordík, Z. Trávníček, K. Peszyński, Valves with flow control by synthetic jets. EPJ Web of Conferences 25 01092 (2012). (Experimental Fluid Mechanics 2011, Jičín, Czech Republic).

[ZB19] Z. Broučková, Z. Trávníček, P. Šafařík, Visualization of synthetic jets at higher Stokes numbers. EPJ Web of Conferences 25 01007 (2012). (Experimental Fluid Mechanics 2011, Jičín, Czech Republic).

Publications not indexed in WoS and Scopus

(some of them in Czech language)

Patents

[ZB20] Z. Trávníček, Z. Broučková, Method and device for cooling of cylinder-shaped bodies by a cooling fluid jet). Patent No. 306506, Jan. 4, 2017 (in Czech).

[ZB21] Z. Trávníček, Z. Broučková, Method and device for generation of a synthetic jet or a hybrid synthetic jet. Patent Application PV 2017-420, June 20, 2017 (in Czech).

Conference contributions

[ZB22] Z. Broučková, Z. Trávníček, Natural convection from a pair of horizontal cylinders at controlled heating. In: Proceedings of 9th World Conference on Experimental Heat Transfer, Fluid Mechanics and Thermodynamics /ExHFT-9/, Iguazu Falls, Brazil, 11-15 June 2017.

[ZB23] Z. Trávníček, F. Maršík, T. Vít, Z. Broučková, M. Pavelka, Lift forces on a circular cylinder in cross flow resulting from heat/mass transfer. In: Proceedings of 16th International Conference on

Computational Methods and Experimental Measurements CMEM 2013, 2 - 4 July, 2013, Coruna, Spain, 149-159.

[ZB24] E. Flídr, P. Šafařík, Z. Trávníček, Z. Broučková, Aktivní řízení proudového pole syntetizovaným proudem v případě příčně obtékaného kruhového válce. Fluid mechanics and thermodynamics - Proceedings of Students' Work in the Year 2015/2016, Eds.: J. Ježek, J. Nožička, J. Adamec, P. Šafařík, ČVUT, Praha, 2016, 41-55.

[ZB25] P. Pušková, P. Šafařík, Z. Trávníček, Z. Broučková, Pasivní řízení symetrického proudu vzduchu. Fluid mechanics and thermodynamics - Proceedings of Students' Work in the Year 2014/2015, Eds.: J. Ježek, J. Nožička, J. Adamec, P. Šafařík, ČVUT, Praha, 2015, 67-79.

[ZB26] E. Flídr, P. Šafařík, Z. Trávníček, Z. Broučková, Malý aerodynamický tunel. Fluid mechanics and thermodynamics - Proceedings of Students' Work in the Year 2014/2015, Eds.: J. Ježek, J. Nožička, J. Adamec, P. Šafařík, ČVUT, Praha, 2015, 33-48.

[ZB27] E. Flídr, P. Šafařík, Z. Trávníček, Z. Broučková, Měření rychlosti a frekvence vzduchu v syntetizovaném proudu. Fluid mechanics and thermodynamics - Proceedings of Students' Work in the Year 2013/2014, Eds.: J. Ježek, J. Nožička, J. Adamec, P. Šafařík, ČVUT, Praha, 2014, 5-17.

[ZB28] I. Ng, V. Timchenko, J. Reizes, Z. Trávníček, J. Kordík, Z. Broučková, Synthetic jets at low Stokes number: numerical and experimental approach. In: 10th International Conference on Flow Dynamics, Sendai International Center, Miyagi, Japan, Nov. 25 - 27, 2013, OS7-8, 472-473.

[ZB29] Z. Trávníček, Z. Broučková, J. Kordík, Visualization of synthetic jet formation in air. In: 12th International Symposium on Fluid Control, Measurement and Visualization (FLUCOME), Nara, Japan, Nov. 18-23, 2013, OS6-02-2.

[ZB30] Z. Broučková, Z. Trávníček, P. Šafařík, Spektrální analýza kontinuálního a syntetizovaného proudu. Fluid mechanics and thermodynamics - Proceedings of Students' Work in the Year 2012/2013, Eds.: J. Ježek, J. Nožička, J. Adamec, P. Šafařík, ČVUT, Praha, 2013, 19-32.

[ZB31] Z. Broučková, Z. Trávníček, P. Šafařík, Vizualizace obtékání rotujícího válce. Fluid mechanics and thermodynamics -

Proceedings of Students' Work in the Year 2011/2012, Eds.: J. Ježek, J. Nožička, J. Adamec, P. Šafařík, ČVUT, Praha, 2012, 19-35.

[ZB32] Z. Trávníček, V. Tesař, Z. Broučková, K. Peszyński, Annular impinging jet controlled by radial synthetic jets. In: 9th International Conference on Heat Transfer, Fluid Mechanics and Thermodynamics, HEFAT 2012, Malta, July 16-18, 2012, 487–493.

[ZB33] Z. Broučková, Z. Trávníček, P. Šafařík, Visualization of the annular synthetic jet. In: Aktuální problémy mechaniky tekutin 2012, Ústav termomechaniky AV ČR, v. v. i.,15.2.–17.2. 2012, str. 13-16.

[ZB34] Z. Broučková, P. Šafařík, Z. Trávníček, Oblast parametrů syntetizovaných proudů. Fluid mechanics and thermodynamics - Proceedings of Student' Work in the Year 2010/2011, Eds.: J. Ježek, J. Nožička, J. Adamec, P. Šafařík, ČVUT, Praha, 2011, 23-38.

[ZB35] Z. Broučková, Z. Trávníček, P. Šafařík, The interaction of continual and synthetic jets. In: Aktuální problémy mechaniky tekutin 2011, Ústav termomechaniky AV ČR, v. v. i.,16.2.–17.2. 2011, str. 21-24.

[ZB36] Z. Broučková, P. Šafařík, Z. Trávníček. Aktivní řízení anulárního proudu radiálním syntetizovaným proudem. Fluid mechanics and thermodynamics - Proceedings of Students' Work in the Year 2009/2010, Eds.: J. Ježek, J. Nožička, J. Adamec, P. Šafařík, ČVUT, Praha, 2010, 5-14.

[ZB37] Z. Broučková, J. Kordík, Z. Trávníček, V. Tesař, P. Šafařík, K. Peszyński, Aktivní řízení anulárního proudu radiálním syntetizovaným proudem. In: Aktuální problémy mechaniky tekutin 2010, Ústav termomechaniky AV ČR, v. v. i.,10.2.–11.2. 2010, str. 23-26.

[ZB38] V. Tesař, Z. Trávníček, J. Kordík, Z. Broučková, Fluidic circuit theory applied to problem of resonant frequency in synthetic-jet actuators. In: 13th International Conference on Developments in Machinery Design and Control, Vol. 11 (2009) pp. 97–98.

Research reports

[ZB39] P. Bauer, Z. Broučková, J. Kordík, M. Sedlář, Návrh metodiky výpočtu ventilačních ztrát převodovky. Výzkumná zpráva Z-1525/15, Ústav termomechaniky AV ČR, 2015.

[ZB40] E. Flídr, Z. Broučková, M. Pavelka, Z. Trávníček, Malý aerodynamický tunel pro vizualizaci proudového pole. Výzkumná zpráva Z-1520/15, Ústav termomechaniky AV ČR, 2015.

[ZB41] Z. Broučková, J. Kordík, Z. Trávníček, Aktivní řízení anulárního proudu radiálním syntetizovaným proudem. Výzkumná zpráva Z 1438/09, Ústav termomechaniky AV ČR, 2009.